Synthesis, Antibacterial Activity, and *In Silico* Analysis of Hydroxyxanthone Derivatives Targeting Gram-Positive and Gram-Negative Bacteria

Enny Fachriyah[1], Muhammad Badrul Huda[1*], Purbowatiningrum Ria Sarjono[1], Faris Hermawan[2], Reinhard Sharon Lase[3], Nanik Wijayati[3], Jumina Jumina[4], Yudhi Dwi Kurniawan[2], and Muhammad Eka Prastya[2]

[1]*Department of Chemistry, Faculty of Science and Mathematics, Diponegoro University, Jl. Prof. Soedharto SH, Tembalang, Semarang 50275, Indonesia*

[2]*Research Center for Pharmaceutical Ingredients and Traditional Medicine, National Research and Innovation Agency (BRIN), KST BJ Habibie, Setu, Tangerang Selatan 15314, Indonesia*

[3]*Department of Chemistry, Universitas Negeri Semarang, Kampus Sekaran, Gunungpati, Semarang 50229, Indonesia*

[4]*Department of Chemistry, Faculty of Mathematics and Natural Sciences, Universitas Gadjah Mada, Sekip Utara, Yogyakarta 55281, Indonesia*

Corresponding author:

tel: +62-82223222661
email: mbadrulhuda@lecturer.undip.ac.id

Received: November 12, 2025
Accepted: January 22, 2026

DOI: 10.22146/ijc.113042

Abstract: *The global rise of antibiotic-resistant bacteria poses a critical health challenge, necessitating the discovery of new antibacterial agents. In this study, three hydroxyxanthone derivatives, 1,5-dihydroxyxanthone (**HX1**), 1,6-dihydroxyxanthone (**HX2**), and 1,7-dihydroxyxanthone (**HX3**) were synthesized in 3.5, 38.2, and 17.54% yields, respectively.* In vitro *assays revealed that all compounds were inactive against* Escherichia coli *(MIC > 1000 μg/mL) but exhibited potent inhibition of* Pseudomonas aeruginosa *(MIC 15.62 μg/mL). Compounds **HX1** and **HX3** also demonstrated strong activity against* Staphylococcus aureus *and* Bacillus subtilis *(MICs of 15.62 μg/mL), while **HX2** showed moderate activity (MIC of 31.25 μg/mL). Molecular docking indicated favorable binding energies (–6.23 to –6.68 kcal/mol) toward DHFR from* E. coli *and* S. aureus*, surpassing those of trimethoprim and tetracycline. Molecular dynamics simulations confirmed stable ligand–protein interactions, and ADMET analyses potential drug-likeness and pharmacokinetic profiles. Overall, **HX1** and **HX3** emerge as promising lead scaffolds for the development of novel DHFR-targeted antibacterial agents against both Gram-positive and Gram-negative pathogens.*

Keywords: *antibacterial; xanthone; synthesis; molecular docking; molecular dynamics*

■ INTRODUCTION

The emergence of antibiotic-resistant bacteria has become a critical global health challenge, resulting in millions of fatalities annually. Projections indicate that by 2030, antibiotic-resistant bacterial infections could be responsible for approximately 5.2 million deaths in the Western Pacific Region [1]. In 2019, *Staphylococcus aureus* was linked to over 1 million deaths, whereas other pathogens, including *Escherichia coli* and *Pseudomonas aeruginosa*, were associated with approximately 500,000 fatalities [2]. *S. aureus* is a highly contagious pathogen responsible for soft tissue, nasal, and skin infections, including cellulitis and furuncles. Additionally, it can cause foodborne illnesses, leading to symptoms such as abdominal pain, vomiting, and nausea [3-4]. *Bacillus subtilis*, a bacterium linked to diarrhea, has demonstrated resistance to both ampicillin and gentamicin [5-6]. *E. coli* causes bloody diarrhea, bacteremia, inflammatory bowel disease, hemorrhagic colitis, hemolytic uremic syndrome, and urinary tract

infections [7]. In contrast, *P. aeruginosa* is responsible for both acute and chronic infections, particularly in immunocompromised individuals with conditions such as chronic obstructive pulmonary disease (COPD), cystic fibrosis, cancer, trauma, burns, sepsis, and ventilator-associated pneumonia (VAP), including cases associated with COVID-19 [8-10]. Therefore, the development of novel antibacterial agents is crucial to addressing global health challenges and achieving the Sustainable Development Goals, ensuring healthy lives and promoting well-being across all age groups.

Xanthones (9*H*-xanthen-9-one) are a class of oxygen-containing heterocyclic compounds distinguished by their symmetrical dibenzo-γ-pyrone core structure [11]. The structural modification of substituents on xanthone rings allows for the development of an extensive range of biological activities, including antimalarial [12-13], anticancer [14-15], antituberculosis [16], antioxidant [17], antifungal [18], and antibacterial [19]. Xanthone derivatives have garnered significant research interest owing to their broad-spectrum antimicrobial properties [20]. Isolated xanthone derivatives are currently under investigation for their potential antimicrobial activity [21-23]. However, their antimicrobial potency is sometimes insufficient, and their isolation and purification processes are labor-intensive and complex. The synthesized xanthone derivatives were also explored for antibacterial activity. Our previous work revealed that 1,3,6-trihydroxyxanthone generated strong antimicrobial activity against *S. aureus* and *E. coli*, with zones of inhibition of 35 and 30 mm, respectively. On the other hand, 1,3-dihydroxyxanthone generated zones of inhibition of 20 and 20 mm against *S. aureus* and *E. coli*, respectively, while 3,6-dihydroxyxanthone generated zones of inhibition of 25 and 30 mm, respectively [24]. A structure-activity relationship (SAR) study of xanthone derivatives conducted by Lu et al. [25] revealed that the carbonyl group within the xanthone skeleton influences antibacterial activity. Additionally, the presence of a hydroxyl substituent at the C3 position has been identified as a critical determinant for enhancing the antibacterial efficacy. Moreover, Bessa et al. [26] reported that the incorporation of an additional hydroxyl group into xanthone compounds enhances their antibacterial activity against *B. subtilis*.

Three hydroxyxanthone derivatives, 1,5-dihydroxyxanthone (**HX1**), 1,6-dihydroxyxanthone (**HX2**), and 1,7-dihydroxyxanthone (**HX3**) were synthesized via a one-pot reaction using Eaton's reagent. Their structures were confirmed by FTIR, MS, and NMR spectroscopies. Antibacterial activities were assessed through MIC and MBC assays against *P. aeruginosa* ATCC 9027, *E. coli* ATCC 8739, *B. subtilis* ATCC 6633, and *S. aureus* ATCC 25923. The potential mechanisms of action were explored through molecular docking, molecular dynamics simulations, and ADMET analyses.

■ EXPERIMENTAL SECTION

Materials

The synthesis of hydroxyxanthones utilizes 2,6-dihydroxybenzoic acid, hydroquinone, resorcinol, 2-methoxyphenol, and Eaton's reagent (P_2O_5/CH_3SO_3H), all of which are of pro-analytical grade and sourced from Sigma Aldrich. Additionally, *n*-hexane, ethyl acetate, methanol, dimethyl sulfoxide (DMSO), distilled water, silica gel for column chromatography, and preparative silica gel were used in the synthesis process. The antibacterial activity was evaluated against a panel of reference bacterial strains obtained from the Research Center for Pharmaceutical Ingredients and Traditional Medicine, National Research and Innovation Agency (BRIN), Indonesia. The tested strains included *P. aeruginosa* ATCC 9027, *E. coli* ATCC 8739, *B. subtilis* ATCC 6633, and *S. aureus* ATCC 25923.

Instrumentation

Hydroxyxanthone derivatives were synthesized using various laboratory instruments, including standard laboratory glassware, a reflux apparatus, a hot plate, a chromatography column, and a reaction chamber. The synthesized compounds were characterized using nuclear magnetic resonance (NMR) spectroscopy (^{1}H-NMR and ^{13}C-NMR, NMR BRUKER ASCEND 700 MHz), a liquid chromatography–mass spectrometry (LC-MS) Shimadzu-QP 2010S, and infrared spectrophotometry (FTIR, Shimadzu Prestige21).

Additionally, antibacterial testing was conducted using a well plate, Petri dishes, a Bunsen burner, an inoculation loop, sealing wrap, and standard laboratory glassware.

Procedure

General procedure for the synthesis of hydroxyxanthones (HX1-HX3)

A reaction mixture comprising 2,6-dihydroxybenzoic acid (2.5 mmol), a substituted phenol (hydroquinone, resorcinol, or 2-methoxyphenol) (2.5 mmol), and Eaton's reagent (2.5 mL) was subjected to heating at 80 °C for 5 h, with reaction progress monitored via thin-layer chromatography (TLC). Upon completion, the reaction mixture was cooled to room temperature and subsequently poured into 25 mL of ice-cold water to facilitate precipitation. The resulting solid was collected via filtration, thoroughly washed with water, and dried under vacuum using a desiccator. The purification process was carried out by chromatographic separation using *n*-hexane and ethyl acetate (1:1 v/v) as eluents to isolate the target compound. The purified products were structurally characterized by FTIR, LC-MS, and NMR spectroscopies to confirm the identity and purity of the synthesized compounds.

1,5-Dihydroxyxanthone (HX1). HX1 was obtained as a yellow solid in 3.5% yield. ^{1}H-NMR (CD_3OD, 700 MHz): δ (ppm) 6.60 (H, ArH_2), 6.62 (H, *d*, ArH_7), 6.72 (H, *dd*, J_4 = 8.8; 2.3 Hz, ArH_4), 6.80 (H, *dd*, J_6 = 8.4; 1.0 Hz, ArH6), 7.47 (H, *t*, J_3 = 8.2 Hz, ArH_3), 7.92 (H, *d*, J_8 = 8.7 Hz, ArH_8). ^{13}C-NMR (CD_3OD, 700 MHz): δ (ppm) 102 (CH_{Ar}, C4), 106 (CH_{Ar}, C8), 108 (CH_{Ar}, C8a), 109 (CH_{Ar}, C2), 111 (CH_{Ar}, C8b), 115 (CH_{Ar}, C6), 126 (CH_{Ar}, C7), 135 (CH_{Ar}, C3), 156 (CH_{Ar}, C4b), 158 (CH_{Ar}, C4a), 161 (C–OH, C6), 168 (C–OH, C1), 181 (C=O, C9). IR (KBr) ν/cm^{-1}: 1038 (C–O),1457 (C=C), 1603 (C=O), 3171 (=C-H sp^2), and 3712 (O–H). MS *m/z* = 229.04 $[M+H]^+$.

1,6-Dihydroxyxanthone (HX2). HX2 was obtained as a yellow solid in a 38.2% yield. ^{1}H-NMR (CD_3OD, 700 MHz): δ (ppm) 6.63 (H, *dd*, J_2 = 8.2; 1.0 Hz, ArH_2), 6.83 (H, *dd*, J_4 = 8.4; 0.9 Hz, ArH_4), 6.71 (H, *d*, J_5 = 2.2 Hz, ArH_5), 6.79 (H, *dd*, J_7 = 8.7; 2.2 Hz, ArH_7), 7.49 (H, *t*, J_3 = 8.3 Hz, ArH_3), 7.98 (H, *d*, J_8 = 8.7 Hz, ArH_8). ^{13}C-NMR (CD_3OD, 700 MHz): δ (ppm) 101 (CH_{Ar}, C5), 106 (CH_{Ar}, C4), 108 (CH_{Ar}, C8a), 109 (CH_{Ar}, C2), 112 (CH_{Ar}, C8b), 113 (CH_{Ar}, C7), 127 (CH_{Ar}, C8), 136 (CH_{Ar}, C3), 156 (CH_{Ar}, C4a), 158 (CH_{Ar}, C4b), 161 (C–OH, C6), 165 (C-OH, C1), 181 (C=O, C9). IR (KBr) ν/cm^{-1}: 1044 (C–O), 1457 (C=C), 1619 (C=O), 3121 (=C–H sp^2), and 3503 (O–H). MS *m/z* = 229.04 $[M+H]^+$.

1,7-Dihydroxyxanthone (HX3). HX3 was obtained as a yellow solid in a 17.54% yield. ^{1}H-NMR (CD_3OD, 700 MHz): δ (ppm) 6.59 (H, *s*, ArH_8), 6.61 (H, ArH_2), 6.72 (H, *dd*, J_6 = 8.8; 2.3 Hz, ArH_6), 6.81 (H, *d*, J_4 = 8.4 Hz, ArH_4), 7.46 (H, *t*, J_3 = 8.3 Hz, ArH_3), 7.91 (H, *d*, J_5 = 8.9 Hz, ArH_5). ^{13}C-NMR (CD_3OD, 700 MHz): δ (ppm) 102 (CH_{Ar}, C4), 106 (CH_{Ar}, C8), 108 (CH_{Ar}, C8a), 109 (CH_{Ar}, C2), 111 (CH_{Ar}, C8b), 115 (CH_{Ar}, C5), 126 (CH_{Ar}, C6), 135 (CH_{Ar}, C3), 156 (CH_{Ar}, C4a), 158 (CH_{Ar}, C4b), 161 (C–OH, C7), 169 (C–OH, C1), 180 (C=O, C9). IR (KBr) ν/cm^{-1}: 1050 (C–O), 1457 (C=C), 1608 (C=O), 2970 (=C–H sp^2), and 3724 (O–H). MS *m/z* = 229.04 $[M+H]^+$.

Antimicrobial activity

The antibacterial efficacy of the samples was evaluated by determining the minimum inhibitory concentration (MIC) and minimum bactericidal concentration (MBC) using the microbroth dilution method [27]. Sample concentrations ranging from 0.78 to 1000 µg/mL were prepared by dilution with methanol p.a. (Sigma) and dispensed into a sterile 96-well plate (Biologix). The prepared samples were mixed with Mueller–Hinton broth (MHB; Oxoid) to a final volume of 100 µL. After cultivation of the bacterial samples for 24 h, 100 µL of each test culture was adjusted to a McFarland standard of 0.5 using 0.85% NaCl (Merck), corresponding to 10^8 CFU/mL. This preparation was then added to each well and incubated for 24 h in a shaker incubator at 150 rpm at 37 °C. Tetracycline (Sigma) and methanol were used as the positive and negative controls, respectively. The MIC value is characterized by the clarity (visible view) of the lowest concentration that represents it. The MBC value was derived from the lowest concentration of the sample that could kill all bacterial cells. The procedure involved applying MIC and higher-concentration treatments to Mueller-Hinton agar (MHA; Oxoid). The absence of bacterial growth at these concentrations indicates the MBC values.

Molecular docking study

The RSCB Protein Data Bank (www.rcsb.org) provided the crystal structures of the DHFR *S. aureus* (PDB ID: 2W9H) and DHFR *synthase* (PDB ID: 6XG5) complexes. Using Chimera software, the protein and native ligand structures were generated and saved as PDB files [28]. The hydroxyxanthone structures were drawn in Avogadro, then optimized using ORCA with the DFT B3LYP/3-21G method, and saved in .pdb format [29]. Molecular docking and redocking were performed using AutoDock4. For *S. aureus* DHFR, a grid box of 30 × 30 × 30 Å was defined with the grid center positioned at (7.358, −5.098, 16.156) along the x, y, and z axes, respectively. For DHFR synthase, a 25 × 25 × 25 Å grid box was employed, centered at (−7.320, 28.052, 18.699). The Lamarckian Genetic Algorithm method was utilized for 50 runs, and the resulting docking outcomes were visualized using Discovery Studio Visualizer (DSV) 2019 [30-31].

Molecular dynamics simulation

Molecular dynamics (MD) simulations of halogenated thioxanthones were performed using GROMACS 2023 software [32-33]. The structural topology of DHFR *S. aureus* was created using the CHARMM36 force field, whereas the topological parameters for all compounds were generated using the CHARMM General Force Field (CGenFF) server (cgenff.com) [34]. Under periodic boundary conditions, the protein-ligand complexes were confined within a cubic simulation box, hydrated with approximately 11,508 water molecules, and neutralized with sodium ions. To confirm system stability before additional simulations, energy minimization was performed for 1 ns using the steepest descent method, and the process terminated when the energy convergence criterion of 10 kJ/mol was met. To establish system stability under regulated thermodynamic conditions of 300 K and 1 atm, a two-step sequential equilibration process was performed, with each phase lasting 100 ps. The equilibration process began with the NVT ensemble, which maintained constant particle number, volume, and temperature, followed by the NPT ensemble, which controlled particle number, pressure, and temperature. The modified Berendsen thermostat, which integrates the v-rescale and c-rescale approaches, was used for temperature and pressure coupling [35-36]. Using the Particle Mesh Ewald approach, electrostatic interactions across vast distances were efficiently calculated while maintaining system homogeneity [37]. The MD simulation was then performed for 100 ns, maintaining a steady temperature of 300 K and a pressure of 1 bar. To assess system stability and conformational changes, MD simulation results were quantitatively examined using graphical representations of the root mean square deviation (RMSD), radius of gyration (Rg), and root mean square fluctuation (RMSF).

MM-PBSA binding free energy analysis

The binding free energy calculations were performed using the g_mmpbsa package, in strict accordance with the methodology reported by Kumari et al. [38]. Equilibrated MD trajectories of each protein–ligand complex, together with their corresponding parameterized topology files, were employed to perform single-trajectory MM-PBSA calculations. This approach enabled a rigorous, quantitative evaluation of binding free energies, thereby providing reliable estimates of the interaction affinities between the ligands and the DHFR receptor.

ADMET prediction

The optimized structures of hydroxyxanthones (**HX1**–**HX3**) were initially prepared in PDB format and subsequently converted to SMILES format using DSV. Following this conversion, each molecular structure was individually submitted to the pkCSM web server for computational analysis [39]. The physicochemical and ADMET parameters were selected using the ADMET menu. Subsequently, the pkCSM server generated a comprehensive dataset for each compound, including an evaluation of compliance with Lipinski's Rule of Five detailed insights into absorption, distribution, metabolism, excretion, and toxicity profiles.

■ RESULTS AND DISCUSSION

Synthesis of Hydroxyxanthone Derivatives

In this study, three hydroxyxanthones were synthesized by the reaction of thiosalicylic acid with

phenol derivatives (2a–c) using Eaton's reagent as the catalyst (Scheme 1). The synthesis of hydroxyxanthone derivatives yielded yellow solid products via a one-pot reaction, with yields of 3.5, 38.2, and 17.54% for **HX1**, **HX2**, and **HX3**, respectively. All hydroxyxanthones were characterized using FTIR, LC-MS, ^{1}H-, and ^{13}C-NMR.

The FTIR spectra of hydroxyxanthones revealed several characteristic absorption bands. The hydroxyl (O–H) stretching vibrations were observed in the range of 3503–3724 cm^{-1}, while the aromatic C=C stretching appeared at 1457 cm^{-1}. The successful formation of the xanthone framework was confirmed by FTIR analysis, which showed characteristic absorption bands for the C=O and C–O–C functional groups at 1603–1609 and 1038–1050 cm^{-1}, respectively. The molecular weights of the synthesized hydroxyxanthones were confirmed using mass spectrometry (MS). Molecular ion peaks corresponding to protonated $[M+H]^{+}$ species for **HX1**, **HX2**, and **HX3** were detected at *m/z* 229. The ^{1}H- and ^{13}C-NMR spectra provide additional evidence for the successful synthesis of hydroxyxanthones. The ^{1}H-NMR spectra of compounds **HX1**–**HX3** exhibited characteristic proton signals within the chemical shift range of 6.59–7.91 ppm, confirming the presence of six aromatic protons. The ^{13}C-NMR spectra of **HX1**–**HX3** confirmed the presence of 13 carbon atoms. The characteristic carbonyl signals of hydroxyxanthones **HX1**, **HX2**, and **HX3** were observed at 181, 181, and 180 ppm, respectively. These spectroscopic data revealed that **HX1**, **HX2**, and **HX3** were successfully synthesized in this study.

In Vitro Antibacterial Assay

The antibacterial activity of **HX1**–**HX3** was evaluated against *E. coli*, *P. aeruginosa*, *S. aureus*, and *B. subtilis* using MIC and MBC assays (Table 1). All compounds were inactive against *E. coli* (MIC > 1000 µg/mL), indicating limited efficacy against this Gram-negative strain, possibly due to the outer membrane's impermeability, which restricts compound penetration. Conversely, all hydroxyxanthones exhibited pronounced inhibitory activity against *P. aeruginosa* (MIC = 15.62 µg/mL). Among them, **HX1** demonstrated the strongest bactericidal effect, with an MBC of 15.62 µg/mL, which was twofold lower than that of **HX2** and **HX3** (31.25 µg/mL). For Gram-positive strains, **HX1** and **HX3** exhibited potent activity against *S. aureus* and *B. subtilis* (MIC = 15.62 µg/mL), whereas **HX2** showed weaker inhibition (MIC = 31.25 µg/mL). Consistent with MIC results, **HX1** displayed the most potent bactericidal effects, with MBC values of 15.62 µg/mL against *S. aureus* and 31.25 µg/mL against *B. subtilis*, which were markedly lower than those of **HX2** (> 62.5 µg/mL) and **HX3** (31.25 µg/mL). These findings indicate that **HX1** possesses the highest antibacterial potency among the synthesized analogues.

Compared with reference compounds, the hydroxyxanthones showed stronger inhibitory activity against *P. aeruginosa* than 3-hydroxyxanthone and 4-hydroxyxanthone, and their effects were comparable to tetracycline against Gram-positive bacteria. The enhanced potency of **HX1** and **HX3** may arise from the favorable positioning of hydroxyl groups at the 1,5- and 1,7-positions, which could enhance hydrogen bonding and increase lipophilicity, facilitating better interaction with bacterial targets or membrane permeability. Overall, these results highlight **HX1** and **HX3** as the

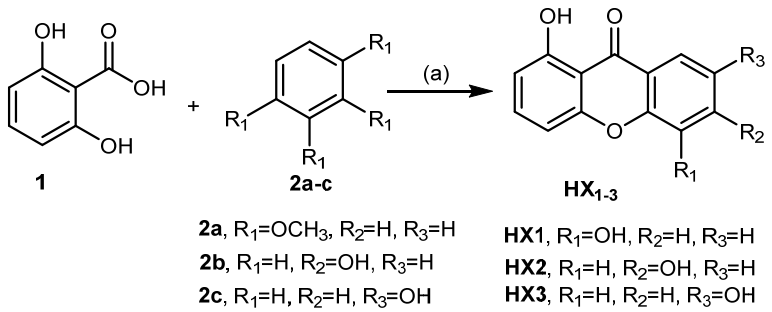

Scheme 1. Synthesis of hydroxyxanthone derivatives **HX1**–**HX3**: (a) Eaton's reagent (2.5 mL)

Table 1. The MIC and MBC values of hydroxyxanthone derivatives

Compound	MIC (μg/mL)				Reference
	E. coli	*P. aeruginosa*	*S. aureus*	*B. subtilis*	
1,5-Dihydroxyxanthone (**HX1**)	> 1000	15.62	15.62	15.62	This work
1,6-Dihydroxyxanthone (**HX2**)	> 1000	15.62	31.25	31.25	This work
1,7-Dihydroxyxanthone (**HX3**)	> 1000	15.62	15.62	15.62	This work
Tetracycline	0.78	0.78	0.78	0.78	This work
3-Hydroxyxanthone	125	-	62.50	-	[40]
4-Hydroxyxanthone	> 256	> 256	64	64	[26]
Trimethoprim	0.5	4.0	4.0	2.0	[41]
Compound	MBC (μg/mL)				Reference
	E. coli	*P. aeruginosa*	*S. aureus*	*B. subtilis*	
HX1	> 1000	15.62	15.62	31.25	This work
HX2	> 1000	31.25	> 62.5	> 62.5	This work
HX3	> 1000	31.25	> 31.25	31.25	This work
Tetracycline	0.78	1.56	0.78	0.78	This work

Table 2. Molecular docking results of the synthesized all hydroxyxanthones

Compound	DHFR *E. coli*		DHFR *S. aureus*	
	Binding energy (kcal/mol)	H-bond	Binding energy (kcal/mol)	H-bond
HX1	−6.23	Ala7, Tyr100	−6.32	Ala7
HX2	−6.29	Asp27, Thr46	−6.41	Ala7
HX3	−6.37	Ala7, Asp27, Tyr100	−6.68	Ala7, Asp27
Tetracycline	−8.30	Ile5, Ala7, Asp27, Ser49, Ile94	−7.73	Leu5, Asp27, Phe92
Trimethoprim	−6.84	Ile5, Asp27, Ser49, Ile94	−7.19	Ile14, Asp27, Phe92

most promising candidates for further antibacterial development.

Molecular Docking Study

Molecular docking was performed to elucidate the potential mechanism of the antibacterial activity of the synthesized **HX1**–**HX3** by inhibiting DHFR from *E. coli* and *S. aureus*. The reliability of the docking protocol was validated by redocking the native ligand trimethoprim into the active site of DHFR, yielding RMSD values of 0.97 Å for *E. coli* and 1.99 Å for *S. aureus*, confirming the accuracy of the docking parameters (RMSD < 2 Å). As RMSD values below 2 Å indicated a reliable and reproducible docking protocol, these findings confirmed the validity of the docking parameters employed [42]. Subsequently, trimethoprim exhibited a lower binding energy for DHFR from *S. aureus* (−7.19 kcal/mol) compared to DHFR from *E. coli* (−6.84 kcal/mol). The findings of this docking study align with those reported by Ali Salman et al., who demonstrated that trimethoprim effectively inhibited DHFR from *E. coli* and *S. aureus*. Nonetheless, *in vitro* studies by Ali Salman et al. [41] demonstrated that trimethoprim is highly active against *E. coli*, suggesting the possibility of an additional mode of action against Gram-negative bacteria, in addition to DHFR inhibition.

As summarized in Table 2, the binding affinities of the hydroxyxanthones toward DHFR *E. coli* ranged from −6.23 to −6.37 kcal/mol, while those for DHFR *S. aureus* were slightly stronger, ranging from −6.32 to −6.68 kcal/mol. This trend aligns with the in vitro findings: all compounds were inactive against *E. coli* (MIC > 1000 μg/mL), whereas they showed significant inhibitory activity against *S. aureus* and *B. subtilis* (MIC 15.62–31.25 μg/mL). The lower binding energies toward *S. aureus* DHFR thus support the observed selectivity for

Gram-positive bacteria. Subsequently, compared with trimethoprim and tetracycline, all tested compounds exhibited higher binding energies, indicating that the hydroxyxanthones had weaker inhibitory potential than trimethoprim and tetracycline. These findings were similar to the *in vitro* results, which showed that all hydroxyxanthones had MICs higher than those of trimethoprim and tetracycline.

Among the hydroxyxanthone derivatives, **HX3** showed the most favorable binding affinity to *S. aureus* DHFR (−6.68 kcal/mol), consistent with its strong *in vitro* antibacterial activity (MIC = 15.62 µg/mL, MBC = 31.25 µg/mL). Compound **HX1** exhibited similar antibacterial potency (MIC = 15.62 µg/mL), consistent with its comparable binding energy (−6.32 kcal/mol). Compound **HX2**, on the other hand, displayed slightly weaker binding energy (−6.41 kcal/mol) and reduced antibacterial activity (MIC = 31.25 µg/mL). These observations indicate that the number and position of hydroxyl substituents on the xanthone ring significantly influence hydrogen-bonding capacity and interaction stability within the DHFR active site, thereby modulating biological activity. The 2D-interaction analysis is shown in Fig. 1 and 2. Trimethoprim, the reference DHFR inhibitor, formed multiple stabilizing hydrogen bonds with key catalytic residues, including Ile5, Asp27, Ser49, and Ile94, in *E. coli* DHFR and Leu5, Asp27, and Phe92 in *S. aureus*, consistent with its potent antibacterial activity (MIC = 0.5 µg/mL) [41]. Tetracycline, which exhibited the most favorable binding energy (−8.30 kcal/mol for *E. coli* and −7.73 kcal/mol *S. aureus*), also engaged in extensive hydrogen bonding and π-alkyl interactions, reflecting its broad-spectrum potency. In contrast, the hydroxyxanthones interacted with fewer active-site residues. **HX3** with the lowest binding energy value formed with Ala7, Asp27, and Tyr100 in π-sulfur and π-alkyl interactions with Met20 and interacts with Asp27 via π-anion interactions. Furthermore, van der Waals interactions occur between Ile5, Ala6, Ile14, Leu28, Trp30, Phe31, Thr46, Ile50, Ile94, Gly95, Gly96,

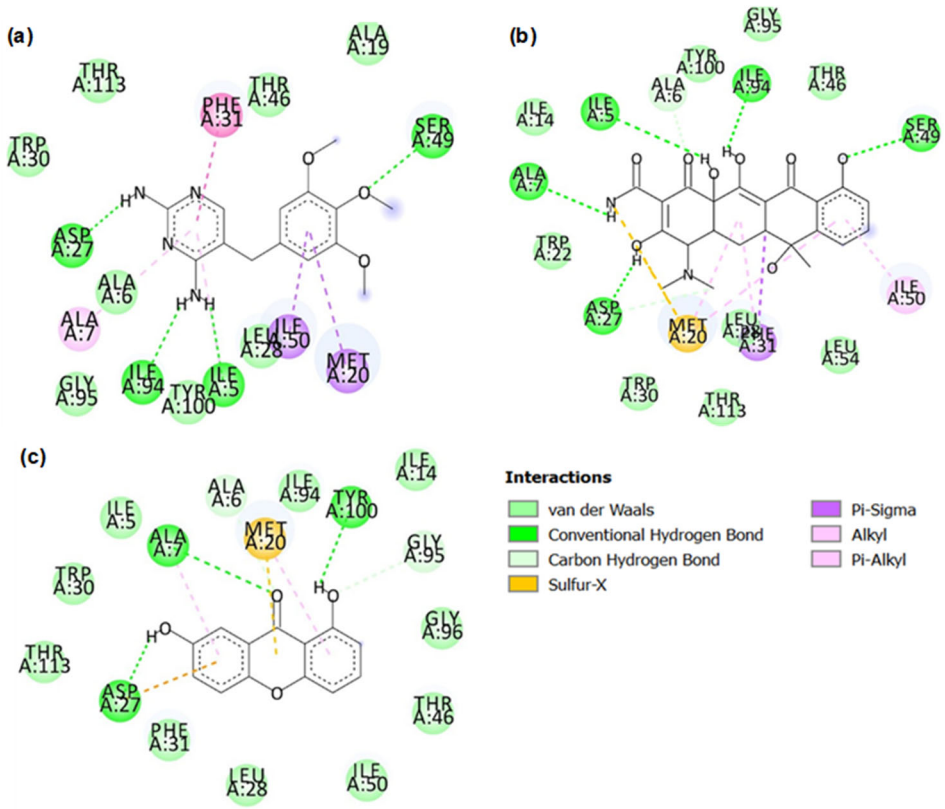

Fig 1. The visualization of non-covalent interactions of (a) trimethoprim, (b) tetracycline, and (c) **HX3** in the active site of DHFR *E. coli*

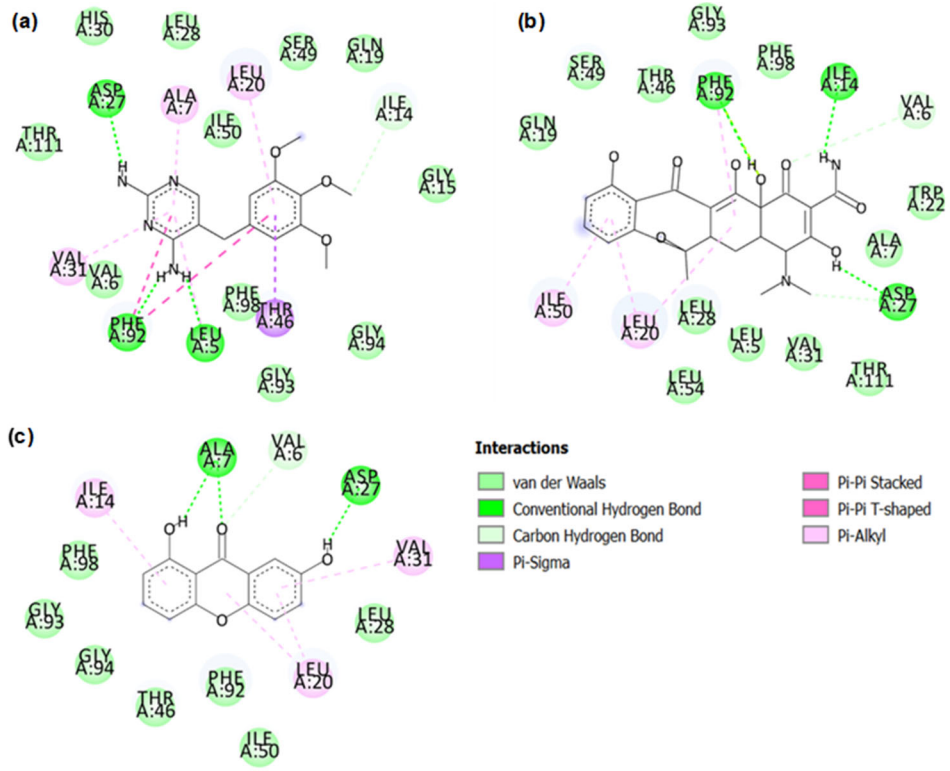

Fig 2. The visualization of non-covalent interactions of (a) trimethoprim, (b) tetracycline, and (c) **HX3** in the active site of DHFR *S. aureus*

and Thr113. Additionally, tetracyline interacted more with Ile5, Ala7, Asp27, Ser49, and Ile94, while trimethopim with Ile5, Asp27, Ser49, and Ile94. Therefore, it could be the reason why the hydroxyxanhtones gave weaker binding energy (−6.37 kcal/mol) than the trimethoprim (−6.84 kcal/mol) and tetracycline (−8.30 kcal/mol). Compounds **HX1** and **HX2** also formed hydrogen bonds with residues Ala7, Asp27, Thr46, and Tyr100, which are located in the substrate-recognition region of DHFR. Although these interactions were less extensive than those of the standard drugs, their orientation within the binding pocket suggests that the xanthone scaffold is capable of mimicking key pharmacophoric features essential for DHFR inhibition.

In the active site of DHFR *S. aureus*, hydroxyxanthone **HX3** interacts with Ala7 and Asp27 through conventional hydrogen bonds; with Ile14, Leu20, and Val31 through pi-alkyl bonds; and with Val6, Leu28, Thr46, Ile50, Phe92, Gly93, Gly94, and Phe98 through van der Waals interactions (Fig. 2). Additionally, tetracycline showed more hydrogen interactions with Leu5, Asp27, and Phe92; and trimethorphyrin with Ile14, Asp27, and Phe92. Therefore, it could be the reason why the hydroxyxanhtones gave a weaker binding energy (−6.68 kcal/mol) than trimethoprim (−7.19 kcal/mol) and tetracycline (−7.73 kcal/mol).

MD Simulation

MD simulations were performed to evaluate the stability and dynamic behavior of **HX1**–**HX3** within the active site of *S. aureus* DHFR. The RMSD profiles of all ligands (Fig. 3(a)) remained within 0.33–1.75 Å, indicating that each compound maintained a stable conformation throughout the 100 ns simulation, with minimal positional deviation from the initial docking pose. The low RMSD values confirm the structural robustness of the complexes and the reliability of the predicted binding orientations [42]. Among the reference inhibitors, trimethoprim and tetracycline exhibited the most stable ligand trajectories, consistent with their strong affinity and potent *in vitro* antibacterial activity.

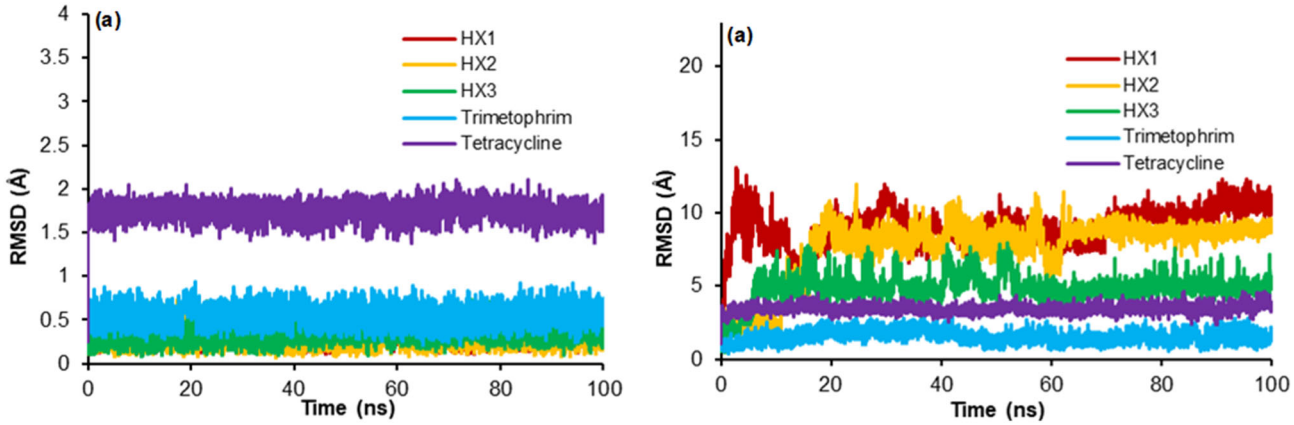

Fig 3. RMSD (a) ligand and (b) complex for **HX1**–**HX3**, tetracycline, trimethoprim

The RMSD of the protein–ligand complexes (Fig. 3(b)) further supported these findings, with average values following the order: trimethoprim (1.54 Å) < tetracycline (3.43 Å) < **HX3** (4.87 Å) < **HX1** ≈ **HX2**. The smaller deviations for trimethoprim and tetracycline reflect stronger and more persistent interactions with the DHFR active site [43]. Among the hydroxyxanthones, **HX3** showed the lowest RMSD, suggesting greater conformational stability and stronger binding than **HX1** and **HX2**, which exhibited greater fluctuations and lower stability. These dynamic observations align well with the docking and *in vitro* results, reinforcing that the enhanced stability of **HX3** within the DHFR binding pocket underlies its superior antibacterial potency and that hydroxyl substitution patterns critically influence the binding stability and biological activity of hydroxyxanthones.

The RMSF is an important parameter for assessing the flexibility and dynamic behavior of a protein structure during MD simulations. Higher RMSF values indicate regions with greater conformational mobility, whereas lower values indicate more structurally constrained, stable regions [44]. The RMSF profile displayed in Fig. 4(a) indicates that compounds **HX1**–**HX3** exhibited amino acid fluctuation patterns similar to those of tetracycline and trimethoprim, with average RMSF values below 2 Å. These findings suggested that the residues surrounding the ligand-binding site revealed minimal structural perturbation, maintaining a relatively stable conformation throughout the simulation [45]. Analysis of the Rg demonstrated that all ligand-bound complexes maintained stable Rg values with minimal fluctuations (Fig. 4(b)). This observation suggested that the protein preserved its structural compactness without undergoing significant conformational expansion.

Collectively, the MD results confirm that all hydroxyxanthones maintain stable interactions within the *S. aureus* DHFR binding cavity over the course of the

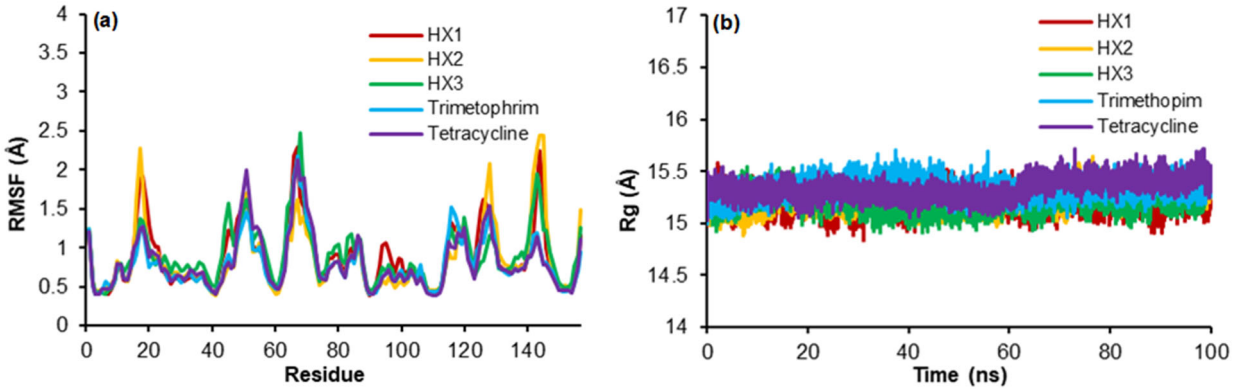

Fig 4. (a) RMSF and (b) Rg for **HX1**–**HX3**, tetracycline, and trimethoprim

simulation. The lower RMSD values and reduced conformational drift of **HX3** highlight its enhanced structural adaptability and interaction stability, providing molecular evidence for its comparatively stronger antibacterial activity. When integrated with the docking and *in vitro* findings, the MD simulations reinforce the conclusion that DHFR inhibition contributes significantly to the antibacterial mechanism of the hydroxyxanthone derivatives.

MM-PBSA Binding Free Energy Analysis

The MM-PBSA binding free energy analysis indicates that the xanthone derivatives **HX1**–**HX3** exhibit consistently favorable binding affinities toward DHFR *S. aureus* (−15.92 to −16.88 kcal/mol), predominantly driven by strong van der Waals interactions, with complementary electrostatic contributions, thereby reflecting stable, well-defined interactions within the enzyme active site (Table 3). This favorable energetic profile is in good agreement with their moderate antibacterial activities against *P. aeruginosa*, *S. aureus*, and *B. subtilis*, as evidenced by MIC values largely ranging from 15.62 to 31.25 μg/mL, suggesting that inhibition of DHFR plays a meaningful role in bacterial growth suppression. Within this series, **HX1** and **HX3** display a more balanced interaction energy landscape accompanied by comparatively lower MIC values, supporting a positive correlation between the predicted binding affinities and the experimentally observed antibacterial potencies among these structurally related compounds. In contrast, tetracycline, despite exhibiting a less favorable MM-PBSA binding free energy toward DHFR (−12.84 kcal/mol) relative to the **HX** derivatives, shows substantially superior antibacterial efficacy (MIC = 0.78 μg/mL across all tested strains), which can be attributed to its efficient intracellular accumulation and well-established multi-target mechanism of action rather than a sole reliance on DHFR inhibition [37].

ADMET Properties

ADMET analysis was conducted to further evaluate the drug-likeness and pharmacokinetic properties of hydroxyxanthone derivatives (Table 4). According to Lipinski's Rule of Five, all hydroxyxanthones comply with established criteria, including a molecular weight not exceeding 500 g/mol, a log P value below 5, a topological polar surface area (TPSA) of less than 140 $Å^2$, and a hydrogen bond donor and acceptor count not exceeding five [46]. The Caco-2 assay is widely used as an *in vitro* model of human intestinal mucosa to assess the absorption potential of orally administered drugs. A compound is classified as having high Caco-2 permeability if its permeability value exceeds 0.90 [47]. All the compounds had a Caco-2 value greater than 0.9. The intestinal absorption (IA) parameter estimates the percentage of drug absorption in the human intestine, with values below 30% indicating poor absorption and those above 80% indicating high absorption [48]. All hydroxyxanthones had IA values > 80%, indicating that they were readily absorbed.

The volume of distribution (VDss) reflects drug distribution in the body; values of log VDss < −0.15 indicate low tissue distribution. All hydroxyxanthones have VDss values above this threshold, suggesting a preference for tissue distribution over plasma [49]. The blood-brain barrier (BBB) permeability of all hydroxyxanthones is below 0.3, and their central nervous

Table 3. MM-PBSA binding energy of ligand trimethoprim, tetracycline, and compounds **HX1**, **HX2**, and **HX3** toward DHFR *S. aureus* protein

Compound	Energy terms (kcal/mol)						
	van der Waal's	Electrostatic	Polar solvation	Nonpolar solvation	Gas-phase free energy	Solvation free energy	Binding energy
HX1	−28.42	−11.51	25.96	−2.91	−39.93	23.05	−16.88
HX2	−23.36	−11.20	21.53	−2.89	−34.56	18.64	−15.92
HX3	−24.44	−9.41	20.33	−2.81	−33.85	17.52	−16.33
Trimethoprim	−31.20	−28.22	41.44	−4.12	−59.42	37.33	−22.09
Tetracycline	−36.54	0.02	27.98	−4.29	−36.52	23.69	−12.84

Table 4. ADMET results of hydroxyxanthones **HX1**–**HX3**

	Properties	Compound		
		HX1	**HX2**	**HX3**
Physicochemical	Molecular weight	228.203	228.203	228.203
	log P	2.3574	2.3574	2.3574
	Rotatable bond	0	0	0
	H-bond acceptor	4	4	4
	H-bond donor	2	2	2
	Surface area	95.35	95.35	95.35
Absorption	Caco-2 permeability	1.016	1.041	1.041
	Intestinal absorption	96.71	95.251	95.251
	Skin permeability	−2.781	−2.735	−2.735
Distribution	VDss	0.045	0.03	0.03
	BBB permeability	0.025	0.048	0.048
	CNS permeability	−2.038	−2.086	−2.086
Metabolism	CYP2D6 substrate	No	No	No
	CYP3A4 substrate	No	No	No
	CYP2D6 inhibitor	No	No	No
	CYP3A4 inhibitor	No	No	No
Excretion	Total clearance	0.105	0.147	0.074
	Renal OCT2 substrate	No	No	No
Toxicity	hERG I inhibitor	No	No	No
	hERG II inhibitor	No	No	No
	Hepatoxicity	No	No	No
	Skin sensitization	No	No	No

system (CNS) permeability is below −2, indicating that these compounds are unlikely to penetrate the blood-brain and central nervous system barriers [50]. None of the hydroxyxanthone derivatives were identified as substrates or inhibitors of CYP2D6 and CYP3A4 enzymes. Subsequently, the excretion data indicated that none of the hydroxyxanthones exceeded the Renal Organic Cation Transporter 2 (OCT2) threshold, yet their total clearance values ranged from 0.074 to 0.147. None of the hydroxyxanthones exhibited inhibitory effects on hERG I or hERG II, suggesting a lack of cardiotoxicity and low risk of inducing cardiac arrhythmia. Furthermore, hepatotoxicity, which is linked to liver damage, was not observed in any of the predicted values, indicating no adverse effects on liver function. Additionally, none of the compounds demonstrated any potential for skin sensitization.

■ CONCLUSION

Three hydroxyxanthone derivatives were successfully synthesized with yields of 3.5, 38.2, and 17.54%, respectively. Their chemical structures were confirmed by FTIR, MS, and NMR. The *in vitro* antibacterial assay showed that none of the hydroxyxanthones exhibited inhibitory activity against *E. coli*, as indicated by MICs exceeding 1000 μg/mL. Conversely, these compounds displayed an MIC of 15.62 μg/mL against *P. aeruginosa*. Furthermore, **HX1** and **HX3** exhibited MIC values of 15.62 μg/mL against *S. aureus* and *B. subtilis*, whereas **HX2** showed a higher MIC value of 31.25 μg/mL. The MBC values of **HX1**–**HX3** range from 15.62–1000 μg/mL. The molecular docking analysis revealed that the binding energies of **HX1**–**HX3** ranged from −6.23 to −6.37 kcal/mol for DHFR *E. coli* and from −6.32 to −6.68 kcal/mol for DHFR *S. aureus*. These values are higher than those observed for trimethoprim and tetracycline. The 100-ns MD simulation demonstrated that **HX1**–**HX3** maintained stability in their interactions with DHFR *E. coli* and DHFR *S. aureus*. However, the RMSD values of tetracycline and trimethoprim were lower than those of **HX1**–**HX3**. Additionally, these compounds conformed to Lipinski's rule of five and fulfilled the essential criteria

for the ADMET property predictions. In conclusion, compounds **HX1** and **HX3** were the most potent antibacterial candidates against *P. aeruginosa*, *S. aureus*, and *B. subtilis*.

■ ACKNOWLEDGMENTS

The authors wish to express their sincere appreciation to the Austrian-Indonesian Center for Computational Chemistry (AIC), Department of Chemistry, Faculty of Mathematics and Natural Sciences, Universitas Gadjah Mada, for generously providing licenses to Gaussian09 and Hyperchem. These resources contributed significantly to the theoretical investigations undertaken in this study. The authors gratefully acknowledge the financial support provided by Diponegoro University through the International Scientific Publication (RPI) LPPM scheme with assignment letter No. 222-484/UN7.D2/PP/IV/2025.

■ CONFLICT OF INTEREST

The authors declare no conflict of interest.

■ AUTHOR CONTRIBUTIONS

Conceptualization, Enny Fachriyah and Muhammad Badrul Huda; Methodology, Enny Fachriyah, Muhammad Badrul Huda, and Purbowatiningrum Ria Sarjono; Software, Faris Hermawan; Validation, Enny Fachriyah, Muhammad Badrul Huda, and Nanik Wijayati; Formal Analysis, Muhammad Badrul Huda and Purbowatiningrum Ria Sarjono; Investigation, Reinhard Sharon Lase, Nanik Wijayati, and Muhammad Eka Prastya; Resources, Jumina and Yudhi Dwi Kurniawan; Data Curation, Faris Hermawan and Reinhard Sharon Lase; Writing – Original Draft Preparation, Muhammad Badrul Huda and Reinhard Sharon Lase; Writing – Review & Editing, Enny Fachriyah, Purbowatiningrum Ria Sarjono, and Yudhi Dwi Kurniawan; Visualization, Faris Hermawan; Supervision, Enny Fachriyah and Jumina; Project Administration, Muhammad Badrul Huda; Funding Acquisition, Enny Fachriyah and Jumina.

■ REFERENCES

[1] World Health Organization, 2023, *Antimicrobial resistance expected to cause 5.2 million deaths in the Western Pacific by 2030*, WHO Regional Office for the Western Pacific, Manila, https://www.who.int/westernpacific/news/item/13-06-2023-antimicrobial-resistance-expected-to-cause-5.2-million-deaths-in-the-western-pacific-by-2030, accessed on October 3, 2025.

[2] GBD 2019 Antimicrobial Resistance Collaborators, 2022, Global mortality associated with 33 bacterial pathogens in 2019: A systematic analysis for the Global Burden of Disease Study 2019, *Lancet*, 400 (10369), 2221–2248.

[3] Howden, B.P., Giulieri, S.G., Wong Fok Lung, T., Baines, S.L., Sharkey, L.K., Lee, J.Y.H., Hachani, A., Monk, I.R., and Stinear, T.P., 2023, *Staphylococcus aureus* host interactions and adaptation, *Nat. Rev. Microbiol.*, 21 (6), 380–395.

[4] Tong, S.Y.C., Davis, J.S., Eichenberger, E., Holland, T.L., and Fowler, V.G., 2015, *Staphylococcus aureus* infections: Epidemiology, pathophysiology, clinical manifestations, and management, *Clin. Microbiol. Rev.*, 28 (3), 603–661.

[5] Haque, M.A., Hu, H., Liu, J., Islam, M.A., Hossen, F., Rahman, M.A., Ahmed, F., and He, C., 2024, Emergence of multidrug-resistant *Bacillus* spp. derived from animal feed, food and human diarrhea in South-Eastern Bangladesh, *BMC Microbiol.*, 24 (1), 61.

[6] Adamski, P., Byczkowska-Rostkowska, Z., Gajewska, J., Zakrzewski, A.J., and Kłębukowska, L., 2023, Prevalence and antibiotic resistance of *Bacillus* sp. isolated from raw milk, *Microorganisms*, 11 (4), 1065.

[7] Pokharel, P., Dhakal, S., and Dozois, C.M., 2023, The diversity of *Escherichia coli* pathotypes and vaccination strategies against this versatile bacterial pathogen, *Microorganisms*, 11 (2), 344.

[8] Rossi, E., La Rosa, R., Bartell, J.A., Marvig, R.L., Haagensen, J.A.J., Sommer, L.M., Molin, S., and Johansen, H.K., 2021, *Pseudomonas aeruginosa* adaptation and evolution in patients with cystic fibrosis, *Nat. Rev. Microbiol.*, 19 (5), 331–342.

[9] Jurado-Martín, I., Sainz-Mejías, M., and McClean, S., 2021, *Pseudomonas aeruginosa*: An audacious

pathogen with an adaptable arsenal of virulence factors, *Int. J. Mol. Sci.*, 22 (6), 3128.

[10] Cendra, M.D.M., and Torrents, E., 2021, *Pseudomonas aeruginosa* biofilms and their partners in crime, *Biotechnol. Adv.*, 49, 107734.

[11] Proença, C., Albuquerque, H.M.T., Ribeiro, D., Freitas, M., Santos, C.M.M., Silva, A.M.S., and Fernandes, E., 2016, Novel chromone and xanthone derivatives: Synthesis and ROS/RNS scavenging activities, *Eur. J. Med. Chem.*, 115, 381–392.

[12] Hastuti, L.P., Hermawan, F., Iresha, M.R., Ernawati, T., and Firdayani, F., 2024, *In-silico* studies of hydroxyxanthone derivatives as potential *pf*DHFR and *pf*DHODH inhibitor by molecular docking, molecular dynamics simulation, MM-PBSA calculation and pharmacokinetics prediction, *Inf. Med. Unlocked*, 47, 101485.

[13] Kurniawan, Y.S., Harizal, H., Yudha, E., Gurning, K., Pranowo, H., Sholikhah, E., and Jumina, J., 2025, Anticancer and antimalarial assays of xanthone–fatty acid hybrids: Integrative *in vitro* and *in silico* evaluation, *Indones. J. Chem.*, 25 (4), 1244–1259.

[14] Kurniawan, Y.S., Yudha, E., Nugraha, G., Fatmasari, N., Pranowo, H., Jumina, J., and Sholikhah, E.N., 2024, Molecular docking and molecular dynamic investigations of xanthone–chalcone derivatives against epidermal growth factor receptor for preliminary discovery of novel anticancer agent, *Indones. J. Chem.*, 24 (1), 250–266.

[15] Iresha, M., Jumina, J., Pranowo, H., Sholikhah, E.N., and Hermawan, F., 2022, Synthesis, cytotoxicity evaluation and molecular docking studies of xanthyl-cinnamate derivatives as potential anticancer agents, *Indones. J. Chem.*, 22 (5), 1407–1417.

[16] Elsaman, T., Mohamed, M.S., Eltayib, E.M., Abdalla, A.E., and Mohamed, M.A., 2021, Xanthone: A promising antimycobacterial scaffold, *Med. Chem.*, 17 (4), 310–331.

[17] Gampa, M., Padmaja, P., Khalivulla, S.I., and Reddy, P.N., 2022, Synthesis and antimicrobial and antioxidant activities of 1,2,3-triazole-tethered xanthone derivatives, *Russ. J. Org. Chem.*, 58 (6), 872–877.

[18] Oriola, A.O., and Kar, P., 2024, Naturally occurring xanthones and their biological implications, *Molecules*, 29 (17), 4241.

[19] Araújo, J., Fernandes, C., Pinto, M., and Tiritan, M.E., 2019, Chiral derivatives of xanthones with antimicrobial activity, *Molecules*, 24 (2), 314.

[20] Liu, X., Shen, J., and Zhu, K., 2022, Antibacterial activities of plant-derived xanthones, *RSC Med. Chem.*, 13 (2), 107–116.

[21] Anggia, V., Bakhtiar, A., and Arbain, D., 2015, The isolation of xanthones from trunk latex of *Garcinia mangostana* Linn. and their antimicrobial activities, *Indones. J. Chem.*, 15 (2), 187–193.

[22] Wang, W., Liao, Y., Huang, X., Tang, C., and Cai, P., 2018, A novel xanthone dimer derivative with antibacterial activity isolated from the bark of *Garcinia mangostana*, *Nat. Prod. Res.*, 32 (15), 1769–1774.

[23] Heilman, D.N.A.A., Hui, A.Y.C., Mian, V.J.Y., Ahmad, F.B., Cee, L.P., Stanslas, J., and Zamakshshari, N.H., 2023, Synthesis and biological evaluation of novel xanthone derivatives with antibacterial potential, *ChemistrySelect*, 8 (46), e202302737.

[24] Yuanita, E., Sudarma, I.M., Sudewiningsih, N.M., Syahri, J., Dharmayani, N.K.T., Sudirman, S., Ulfa, M., and Sumarlan, I., 2020, Antibacterial activity and molecular docking studies of series hydroxyxanthone, *AIP Conf. Proc.*, 2243 (1), 020032.

[25] Lu, Y., Guan, T., Wang, S., Zhou, C., Wang, M., Wang, X., Zhang, K., Han, X., Lin, J., Tang, Q., Wang, C., and Zhou, W., 2023, Novel xanthone antibacterials: Semi-synthesis, biological evaluation, and the action mechanisms, *Bioorg. Med. Chem.*, 83, 117232.

[26] Bessa, L.J., Palmeira, A., Gomes, A.S., Vasconcelos, V., Sousa, E., Pinto, M., and Martins da Costa, P., 2015, Synergistic effects between thioxanthones and oxacillin against methicillin-resistant *Staphylococcus aureus*, *Microb. Drug Resist.*, 21 (4), 404–415.

[27] Hening, E.N.W., Priyanto, J.A., Prastya, M.E., Astuti, R.I., Hasidu, L.O.A.F., and Jamilah, J., 2024, Soil

bacteria from Muna Island, Southeast Sulawesi, Indonesia: Antibacterial and antibiofilm activities, and the presence of antibiotic-biosynthetic genes, *J. Appl. Pharm. Sci.*, 14 (6), 207–217.

[28] Pettersen, E.F., Goddard, T.D., Huang, C.C., Couch, G.S., Greenblatt, D.M., Meng, E.C., and Ferrin, T.E., 2004, UCSF Chimera—A visualization system for exploratory research and analysis, *J. Comput. Chem.*, 25 (13), 1605–1612.

[29] Neese, F., 2018, Software update: the ORCA program system, version 4.0, *WIREs Comput. Mol. Sci.*, 8 (1), e1327.

[30] BIOVIA, Dassault Systèmes, 2019, *Discovery Studio Visualizer v.20.1.0.19295*, Dassault Systèmes, San Diego, US.

[31] Fuhrmann, J., Rurainski, A., Lenhof, H.P., and Neumann, D., 2010, A new Lamarckian genetic algorithm for flexible ligand–receptor docking, *J. Comput. Chem.*, 31 (9), 1911–1918.

[32] Huang, J., Alexander, D., and MacKerell Jr., A.D., 2013, CHARMM36 all-atom additive protein force field: validation based on comparison to NMR data, *J. Comput. Chem.*, 34 (25), 2135–2145.

[33] Hess, B., Kutzner, C., van der Spoel, D., and Lindahl, E., 2008, GROMACS 4: Algorithms for highly efficient, load-balanced, and scalable molecular simulation, *J. Chem. Theory Comput.*, 4 (3), 435–447.

[34] Vanommeslaeghe, K., Raman, E.P., and MacKerell Jr., A.D., 2012, Automation of the CHARMM general force field (CGenFF) II: assignment of bonded parameters and partial atomic charges, *J. Chem. Inf. Model.*, 52 (12), 3155–3168.

[35] Bussi, G., Donadio, D., and Parrinello, M., 2007, Canonical sampling through velocity rescaling, *J. Chem. Phys.*, 126 (1), 014101.

[36] Bernetti, M., and Bussi, G., 2020, Pressure control using stochastic cell rescaling, *J. Chem. Phys.*, 153 (11), 114107.

[37] Darden, T., York, D., and Pedersen, L., 1993, Particle mesh Ewald: An N·log(N) method for Ewald sums in large systems, *J. Chem. Phys.*, 98 (12), 10089–10092.

[38] Kumari, R., Kumar, R., and Lynn, A., 2014, g_mmpbsa—a GROMACS tool for high-throughput MM-PBSA calculations, *J. Chem. Inf. Model.*, 54 (7), 1951–1962.

[39] Pires, D.E.V., Blundell, T.L., and Ascher, D.B., 2015, pkCSM: Predicting small-molecule pharmacokinetic and toxicity properties using graph-based signatures, *J. Med. Chem.*, 58 (9), 4066–4072.

[40] Kurniawan, Y.S., Yudha, E., Jumina, J., Pranowo, H.D., and Sholikhah, E.N., 2025, Synthesis, *in vitro* antimicrobial activity, and *in silico* bioinformatical approach of xanthone–fatty acid esters against *Staphylococcus aureus*, *Escherichia coli*, and *Candida albicans*, *Eur. J. Med. Chem. Rep.*, 13, 100245.

[41] Ali Salman, G., Zinad, D.S., Mahal, A., Rizki Fadhil Pratama, M., Duan, M., Alkhouri, A., and Alamiery, A., 2022, Synthesis and biological evaluation of xanthone derivatives, *ChemistrySelect*, 7 (4), e202103901.

[42] Nivatya, H.K., Singh, A., Kumar, N., Sonam, S., Sharma, L., Singh, V., Mishra, R., Gaur, N., and Mishra, A.K., 2025, Assessing molecular docking tools: Understanding drug discovery and design, *Future J. Pharm. Sci.*, 11 (1), 111.

[43] Aier, I., Varadwaj, P., and Raj, U., 2016, Structural insights into conformational stability of both wild-type and mutant EZH2 receptor, *Sci. Rep.*, 6, 34984.

[44] Hassan, A.M., Gattan, H.S., Faizo, A.A., Alruhaili, M.H., Alharbi, A.S., Bajrai, L.H., AL-Zahrani, I.A., Dwivedi, V.D., and Azhar, E.I., 2024, Evaluating the binding potential and stability of drug-like compounds with the Monkeypox virus VP39 protein using molecular dynamics simulations and free energy analysis, *Pharmaceuticals*, 17 (12), 1617.

[45] Bagewadi, Z.K., Yunus Khan, T.M., Gangadharappa, B., Kamalapurkar, A., Mohamed Shamsudeen, S., and Yaraguppi, D.A., 2023, Molecular dynamics and simulation analysis against superoxide dismutase (SOD) target of *Micrococcus luteus* with secondary metabolites from *Bacillus licheniformis* recognized by genome mining approach, *Saudi J. Biol. Sci.*, 30 (9), 103753.

[46] Lipinski, C.A., Lombardo, F., Dominy, B.W., and Feeney, P.J., 2001, Experimental and computational approaches to estimate solubility and permeability

in drug discovery and development settings, *Adv. Drug Delivery Rev.*, 46 (1-3), 3–26.

[47] Sambuy, Y., De Angelis, I., Ranaldi, G., Scarino, M.L., Stammati, A., and Zucco, F., 2005, The Caco-2 cell line as a model of the intestinal barrier: Influence of cell and culture-related factors on Caco-2 cell functional characteristics, *Cell Biol. Toxicol.*, 21 (1), 1–26.

[48] Radchenko, E.V., Dyabina, A.S., Palyulin, V.A., and Zefirov, N.S., 2016, Prediction of human intestinal absorption of drug compounds, *Russ. Chem. Bull.*, 65 (2), 576–580.

[49] Flores-Holguín, N., Frau, J., and Glossman-Mitnik, D., 2021, Computational pharmacokinetics report, ADMET study and conceptual DFT-based estimation of the chemical reactivity properties of marine cyclopeptides, *ChemistryOpen*, 10 (11), 1142–1149.

[50] Kunwittaya, S., Nantasenamat, C., Treeratanapiboon, L., Srisarin, A., Isarankura-Na-Ayudhya, C., and Prachayasittikul, V., 2013, Influence of logBB cut-off on the prediction of blood–brain barrier permeability, *Biomed. Appl. Technol. J.*, 1, 16–34.